Check for updates

ADVANCED ENERGY MATERIALS
www.advenergymat.de

Phenothiazine-Based Self-Assembled Monolayer with Thiophene Head Groups Minimizes Buried Interface Losses in Tin Perovskite Solar Cells

Valerio Stacchini, Madineh Rastgoo, Mantas Marčinskas, Chiara Frasca, Kazuki Morita, Lennart Frohloff, Antonella Treglia, Thomas W. Gries, Orestis Karalis, Vytautas Getautis, Florian Ruske, Annamaria Petrozza, Norbert Koch, Hannes Hempel, Tadas Malinauskas, Antonio Abate,* and Artem Musiienko**

Self-assembled monolayers (SAMs) have revolutionized the fabrication of lead-based perovskite solar cells, but they still remain underexplored in tin perovskite systems. To date, PEDOT remains the most effective hole-selective layer in tin perovskite solar cells (TPSCs), yet it presents challenges for both performance and stability. MeO-2PACz, the only SAM reported for tin perovskites consistently underperforms when compared to PEDOT. In this work, it is identified that MeO-2PACz's limitations stem from excessively strong interactions with the perovskite surface and poor lattice matching, which leads to inferior interface quality. To address these issues, a novel SAM-forming molecule called Th-2EPT is designed, synthesized, and characterized. Density functional theory (DFT) is used to evaluate coordination strength and lattice compatibility, complemented by electro-optical characterisation techniques that show significantly reduced interfacial recombination and improve material crystallinity in Th-2EPT/Perovskite films. With Th-2EPT, the first SAM-based tin perovskite solar cells that outperform PEDOT-based devices, delivering a power conversion efficiency (PCE) of 8.2% with a DMSO-free solvent system, are demonstrated.

1. Introduction

Thanks to their simple processing, bandgap tunability, and defect tolerance, perovskites are on track to radically change the world of photovoltaics. However, two challenges must be addressed before this technology can be considered competitive for commercialisation: long-term stability and lead toxicity.[1–4] Intense research is focused on developing nontoxic alternatives to mitigate the toxicity issues of lead-containing perovskites.[2,5,6] Tin perovskite solar cells are potentially even more stable than their lead-based counterparts, exhibiting negligible ion migration.[3,7,8] Despite their potential, TPSCs underperform compared to their lead counterparts, hindered by rapid crystallisation and unstable interfaces,[2] due to the facile oxidation

V. Stacchini, C. Frasca, K. Morita, T. W. Gries, O. Karalis, F. Ruske, N. Koch, H. Hempel, A. Abate, A. Musiienko
Solar Energy Division
Helmholtz-Zentrum Berlin für Materialien und Energie GmbH
Hahn-Meitner-Platz 1, 14109 Berlin, Germany
E-mail: antonio.abate@helmholtz-berlin.de; artem.musiienko@helmholtz-berlin.de

V. Stacchini, C. Frasca, T. W. Gries, A. Abate
Department of Chemistry
University of Bielefeld
Universitätsstraße 25, 33615 Bielefeld, Germany

M. Rastgoo, A. Abate
Department of Chemical
Materials and Production Engineering
University of Naples Federico II
Piazzale Tecchio, 80, Naples 80125, Italy

M. Marčinskas, V. Getautis, T. Malinauskas
Department of Organic Chemistry
Kaunas University of Technology
Radvilenu pl. 19, Kaunas LT-50254, Lithuania
E-mail: tadas.malinauskas@ktu.lt

L. Frohloff, N. Koch
Institut für Physik & Center for the Science of Materials (CSMB)
Humboldt-Universität zu Berlin
Newtonstraße 15, 12489 Berlin, Germany

A. Treglia, A. Petrozza
Center for Nano Science and Technology
Istituto Italiano di Tecnologia (IIT)
via Rubattino 81, Milan 20134, Italy

A. Musiienko
Robotized Optoelectronic Material and Photovoltaic Engineering
Helmholtz-Zentrum Berlin für Materialien und Energie (HZB)
12849 Adlershof, Berlin, Germany

The ORCID identification number(s) for the author(s) of this article can be found under https://doi.org/10.1002/aenm.202500841

© 2025 The Author(s). Advanced Energy Materials published by Wiley-VCH GmbH. This is an open access article under the terms of the Creative Commons Attribution License, which permits use, distribution and reproduction in any medium, provided the original work is properly cited.

DOI: 10.1002/aenm.202500841

of Sn^{2+} to Sn^{4+} and poor energy-level alignment between standard selective contacts and the absorber layer.[1,2,8–10]

Until now, in most studies on tin perovskite solar cells, poly(3,4-ethylene dioxythiophene) polystyrene sulfonate, (PEDOT: PSS)serves as the gold-standard hole-selective layer (HSL) in current tin perovskite solar cell. However, the significant energetic misalignment, acidity, and hygroscopicity limit the performance of PEDOT-based devices and lead to device degradation.[2,11–14] Due to the inherent chemical limitations of PEDOT, overcoming its drawbacks calls for the design of novel materials. Self-assembled monolayers (SAMs) are emerging as a key alternative to PEDOT due to their dual role in interface passivation and charge selectivity.[15–17] While SAMs have demonstrated success in lead-based perovskites by improving charge extraction and passivating interfaces, their application in tin perovskites remains underexplored. To the best of our knowledge, MeO-2PACz is the only SAM successfully employed for tin perovskites, achieving moderate power conversion efficiencies (PCEs) of 5.8%[9] and 9.4%,[18] obtained with a DMSO-free and DMSO solvent system, respectively. Regardless of the solvent system, SAM-based solar cells have yet to outperform PEDOT controls, and the underlying causes of poor performance remain unclear.[2,19–21] In this work, we use first-principles calculations to identify the limitations of MeO-2PACz, revealing its strong interaction with the $FASnI_3$ lattice and dimensional mismatch as the cause for a highly defective interface. We employ a DMSO-free solvent system for tin PSCs to mitigate solvent-induced degradation, addressing two key challenges: the oxidation of Sn^{2+} by DMSO and the presence of residual DMSO, which can further promote oxidation over the device's lifetime.

To overcome this incompatibility between the MeO-2PACz and tin perovskite, we design and synthesize a novel SAM molecule, {2-[3,7-di(thiophen-3-yl)-10*H*-phenothiazin-10-yl]ethyl}phosphonic acid or Th-2EPT, featuring two thiophene passivating head groups, a phenothiazine core and a phosphonic acid anchoring group. Th-2EPT significantly improved the interfacial quality of tin perovskites by enhancing lattice matching and fine-tuning interaction strength. This work marks the first successful attempt to fabricate well-functioning SAM-based tin perovskite solar cells. Th-2EPT is able to compete with and outperform PEDOT, thanks to positive chemical interaction, lattice matching and improved optoelectronic properties of perovskite films grown on this SAM.

2. Results and Discussion

To investigate the underperformance of MeO-2PACz in tin perovskite solar cells, we examined its interfacial interaction with the perovskite lattice using density functional theory (DFT). Specifically, we evaluated two key descriptors of interface quality: the binding energy of the SAM to the $FASnI_3$'s uncoordinated Sn^{2+} surface ions and the degree of lattice matching between the SAM's passivating head groups and the perovskite cationic sublattice.

In the case of MeO-2PACz, we simulated the molecule without its phosphonic acid anchor to isolate the interaction of the two methoxy head groups with undercoordinated Sn^{2+} ions. The molecule was fully relaxed on the slab model, and the binding energy was calculated as the interaction energy between the donor atoms and the surface cations (full computational details are provided in the Supporting Information). MeO-2PACz exhibited a high binding energy of 0.45 eV (**Figure 1c**), in line with strong Lewis acid–base adduct formation between its electronegative oxygen atoms and Sn^{2+}. While this strong interaction could be beneficial for anchoring, it may also rigidly lock the interface, preventing the perovskite lattice from undergoing necessary rearrangements during film formation. Previous studies have suggested that strong molecular interactions can sometimes be detrimental, as they may rigidly anchor the interface, hindering the natural rearrangements of the perovskite lattice during crystal growth.[17,22,23]

Next, we evaluated the spatial compatibility between the molecule's O—O spacing (7.81 Å) and the calculated Sn—Sn distances on the perovskite surface (6.53 Å – Figure 1a). The best match was found with the second-nearest neighbors (9.22 Å), corresponding to a rather low 85% match (Figure 1b). A detailed calculation on lattice matching is discussed in the Supporting Information. We hypothesize that, in the case of MeO-2PACz, the combination of strong interactions with undercoordinated Sn^{2+} ions and poor lattice compatibility may induce interfacial strain and promote defect formation.

To address lattice incompatibility of MeO-2PACz, we designed a new SAM molecule, Th-2EPT, with two main objectives: reduce binding strength and improve lattice compatibility. In place of the carbazole core used in MeO-2PACz, we introduced a phenothiazine unit—a well-established, low-cost electron-rich structure.[24–26] To reduce the binding strength observed with methoxy groups, we replaced them with thiophene units, which were introduced at positions 3 and 7 of the phenothiazine core (Figure 1d). Thiophenes were selected due to their lower electronegativity relative to oxygen, while still offering proven effectiveness in surface passivation for both tin- and lead-based perovskites.[27,28] We retained the phosphonic acid anchor, given its proven effectiveness in ensuring robust adhesion.[29,30] The resulting molecular structure, visible in Figure 1d, named diethyl{2-[3,7-di(thiophen-3-yl)-10H-phenothiazin-10-yl]ethyl}phosphonate (Th-2EPT), was investigated with the same DFT methodology. Th-2EPT exhibited a substantially lower binding energy of 0.14 eV (Figure 1f), attributed to the less electronegative sulfur atoms and their more delocalized bonding character. This weaker interaction suggests a more flexible, less disruptive binding mode that could facilitate perovskite crystallization. Geometrically, Th-2EPT showed a near-ideal S—S spacing of 14.01 Å, matching the fifth-nearest Sn—Sn distance in $FASnI_3$ (14.6 Å) with 96% alignment (for detailed calculations, see Supporting Information). The superior geometric match, combined with moderate binding strength, indicates that Th-2EPT could passivate the perovskite surface without introducing strain or defects.

Motivated by the favorable binding energy and lattice compatibility predicted for Th-2EPT, we synthesized the molecule and experimentally tested its effect on $FASnI_3$ film formation (synthetic steps are summarized in Table S1, Supporting Information, followed by a detailed description of the synthetic intermediates). We deposited $FASnI_3$ perovskite on PEDOT, MeO-2PACz and Th-2EPT on ITO substrates. PEDOT was included as a reference in this stage of the study, given its role as the most well-known hole transport layer (HTL) in $FASnI_3$ solar cells.[9,21]

© 2025 The Author(s). Advanced Energy Materials published by Wiley-VCH GmbH

16146840, 2025, 29, Downloaded from https://advanced.onlinelibrary.wiley.com/doi/10.1002/aenm.202500841 by Helmholtz-Zentrum Berlin Für, Wiley Online Library on [02/09/2025]. See the Terms and Conditions (https://onlinelibrary.wiley.com/terms-and-conditions) on Wiley Online Library for rules of use; OA articles are governed by the applicable Creative Commons License

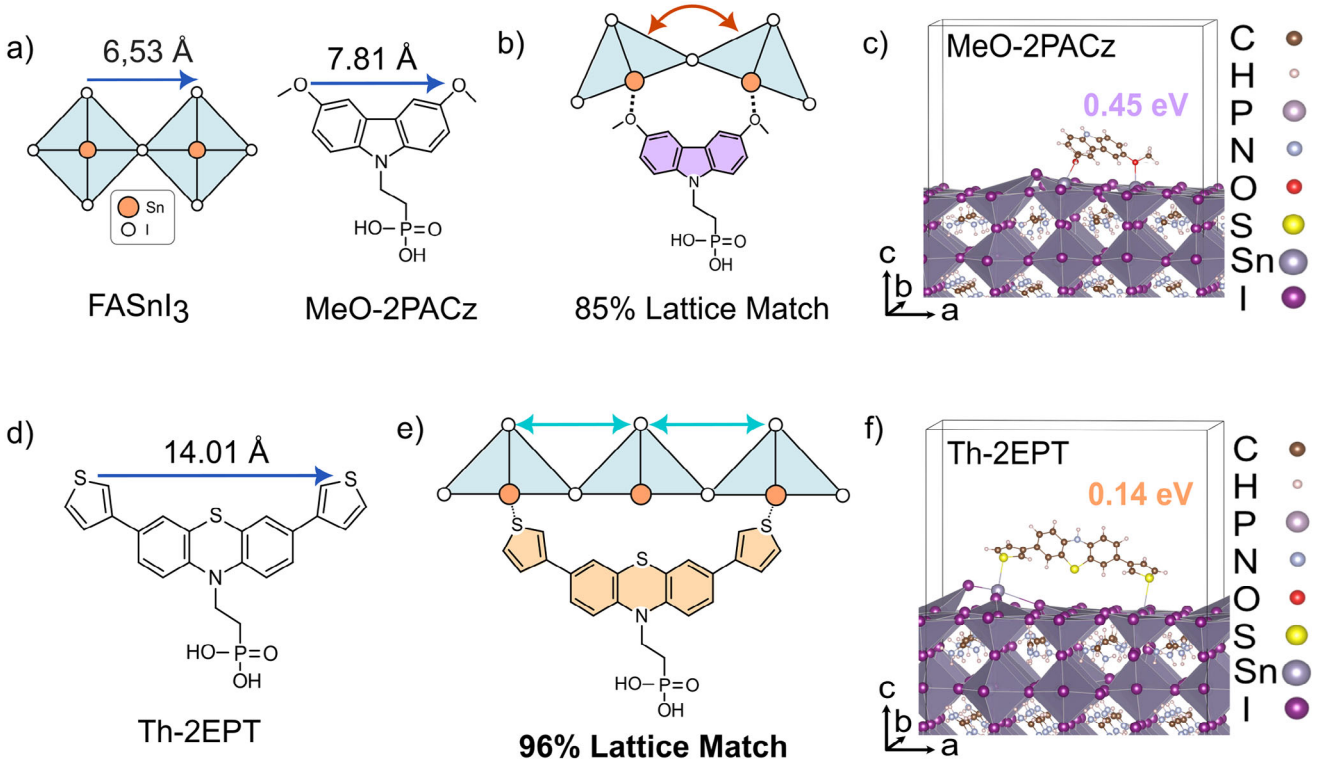

Figure 1. SAM-perovskite interaction and lattice match. a) Structures and characteristic dimensions of FASnI3 lattice and the MeO-2PACz phosphonic acid. b) Graphical representation of lattice mismatch between MeO-2PACz and the FASnI3 lattice. c,f) DFT-calculated binding energies for the two molecules on top of a SnI_2-terminated $FASnI_3$ surface. The values in eV denote the computed binding energies at the interface. d) Molecular structure of Th-2EPT and S-S distance between head groups. e) Lattice matching between Th-2EPT and the FASnI lattice. For graphical clarity, the illustration simplifies the 96% lattice match of Th-2EPT by representing it as alignment with two lattice parameters; the full calculation with fifth-nearest-neighbor matching is provided in the Supporting Information.

PEDOT and MeO-2PACz were spin-coated, while target Th-2EPT was deposited through dip-coating. In the case of PEDOT films, an alumina (Al_2O_3) nanoparticles scaffold is spin-coated between PEDOT and perovskite. This step is necessary to improve the wetting of PEDOT.[21] Contact angle measurements (**Figure 2a–c**) confirmed good wettability for Th-2EPT (69°) and good wettability for PEDOT (59° with the spin-coated alumina nanoparticle wetting layer), and MeO-2PACz (55°). The resulting films were characterized by SEM and XRD to study the film morphology and the effect of the new Th-2EPT SAM on crystallization (Figure 2d,e). XRD shows reflexes from both the ITO substrate and the perovskite layer,[31] and all peaks could be assigned to either of the two materials. XRD diffractograms for the three samples do not exhibit significant differences in the relative intensities of diffraction peaks, suggesting comparable crystallographic orientation across all HTL layers. However, notable differences are observed in the analysis of the primary (100) diffraction peak located ≈14° (Figure 2e). The intensity of this peak is similar for PEDOT and Th-2EPT, whereas it is markedly reduced for MeO-2PACz, indicating lower crystallinity. Peak broadening was evaluated using a Gaussian fitting model, and the full width at half maximum (FWHM) was extracted (more information on the fitting model in the supporting information). The extracted FWHM show a similar trend with respect to the same signal's intensity, with MeO-2PACz showing by far the broadest peak ($FWHM_{MeO}$ = 0.30°) while PEDOT shows the narrowest ($FWHM_{PEDOT}$ = 0.10°), followed by Th-2EPT ($FWHM_{Th\text{-}2EPT}$ = 0.12°). The pronounced peak broadening observed for the film on MeO-2PACz may arise from several factors, including increased microstrain, a higher density of structural defects, reduced crystallinity, or a smaller vertical grain size. Regardless of the dominant mechanism, the broadening indicates a lower structural quality for MeO-2PACz films relative to the films deposited on PEDOT or Th-2EPT. While displaying a very similar FWHM, films on PEDOT and Th-2EPT show a rather different surface morphology in SEM (Figure 2a,c). Films grown on PEDOT exhibit the largest lateral grain size, whereas those deposited on both SAMs display notably smaller and more compact grains. Likely, the grain growth is mainly governed by the usage of an alumina scaffold in the case of PEDOT.

After observing that Th-2EPT significantly improves film crystallinity and morphology—surpassing MeO-2PACz and closely approaching PEDOT—we next investigated how these structural enhancements affect the optoelectronic properties and carrier recombination dynamics of the films. ITO/HTL/Perovskite layer stacks were studied, always illuminating them from the ITO/HTL side, to better probe the buried interface (**Figure 3a**). We employed PLQY, trPL, and TAS measurements to assess how the hole transport layer (HTL) influences radiative efficiency and carrier recombination in perovskite films (Figure 3).

© 2025 The Author(s). Advanced Energy Materials published by Wiley-VCH GmbH

16146840, 2025, 29, Downloaded from https://advanced.onlinelibrary.wiley.com/doi/10.1002/aenm.202500841 by Helmholtz-Zentrum Berlin Für, Wiley Online Library on [02/09/2025]. See the Terms and Conditions (https://onlinelibrary.wiley.com/terms-and-conditions) on Wiley Online Library for rules of use; OA articles are governed by the applicable Creative Commons License

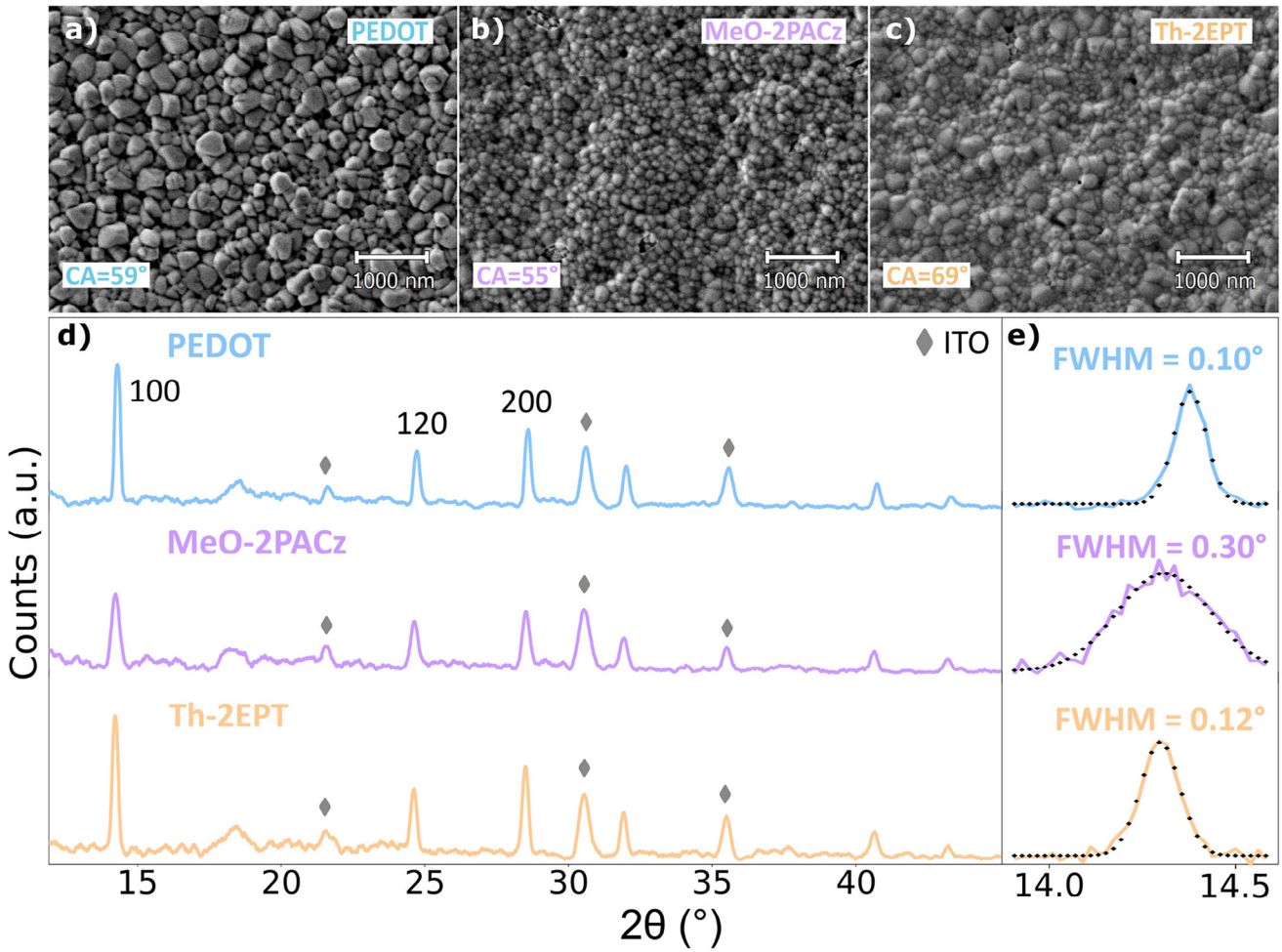

Figure 2. Morphology and crystallinity of perovskite films. a–c) SEM images of perovskite films deposited on PEDOT (a), MeO-2PACz (b), and Th-2EPT (c). Median values for measured contact angles (CA) are indicated (CA data are provided in Figure S8, Supporting Information). d) X-ray diffraction (XRD) patterns of the same films (left), with principal diffraction peaks indexed and ITO substrate peaks marked by diamonds. e) Magnified view of the (100) diffraction peak ≈14°, showing fitted curves (black diamonds) and corresponding full width at half maximum (FWHM) values for each sample, extracted using a Gaussian fitting. More information on the fitting is provided in the Supporting Information.

Figure 3b presents the normalized photoluminescence quantum yield (PLQY) as a function of excitation density for perovskite films deposited on various substrates. At low excitation densities (10^{14} cm^{-3}), the film on Th-2EPT exhibits the highest PLQY, surpassing even that of the reference glass substrate. This elevated PLQY at low carrier concentrations indicates effective suppression of trap-assisted nonradiative recombination, suggesting superior interfacial passivation provided by Th-2EPT. As excitation density increases (10^{16}–10^{17} cm^{-3}), the PLQY values for Th-2EPT, MeO-2PACz, and glass converge, forming a group with similar peak efficiencies. In contrast, the PEDOT-based film consistently displays significantly lower PLQY across the entire excitation range, indicative of higher nonradiative recombination losses and inferior interfacial quality. These observations underscore the efficacy of SAM-based hole transport layers in enhancing radiative recombination efficiency and mitigating interfacial defects. Transient photoluminescence (trPL) was measured on ITO/HTL/Perovskite stacks. The photoluminescence transients reveal clear differences in decay times among the hole transport layers, with Th-2EPT exhibiting the slowest decay (Figure 3c). The trPL data were fitted using a bi-exponential decay model (fitting parameters and corresponding plots are provided in Figure S6, Supporting Information). The resulting fits were then used to compute differential lifetimes according to the expression $t = -\{d\ ln[f(t)]/dt\}^{-1}$, where $f(t)$ is the time-dependent photon flux. In a bi-exponential trPL fit, the fast-decaying exponential models the initial behavior of the decay and is more closely associated with interfacial trap-assisted nonradiative recombination. In contrast, the slowly decaying exponential is more representative of carrier lifetimes.[32,33] Both lifetimes are tabulated in Figure S6 (Supporting Information). While the fast components do not appear in the differential lifetime plots, the slow decay manifests as a plateau in these graphs (Figure 3d). PEDOT reaches this plateau at only 35 ns, indicating the shortest lifetime among the evaluated HTLs, followed by MeO-2PACz with a lifetime of 67 ns. The film on Th-2EPT shows a longer lifetime of 91 ns, while the perovskite grown on quartz exhibits a lifetime of 156 ns—an impressive value when compared to recent studies reporting significantly shorter

© 2025 The Author(s). Advanced Energy Materials published by Wiley-VCH GmbH

16146840, 2025, 29, Downloaded from https://advanced.onlinelibrary.wiley.com/doi/10.1002/aenm.202500841 by Helmholtz-Zentrum Berlin Für, Wiley Online Library on [02/09/2025]. See the Terms and Conditions (https://onlinelibrary.wiley.com/terms-and-conditions) on Wiley Online Library for rules of use; OA articles are governed by the applicable Creative Commons License

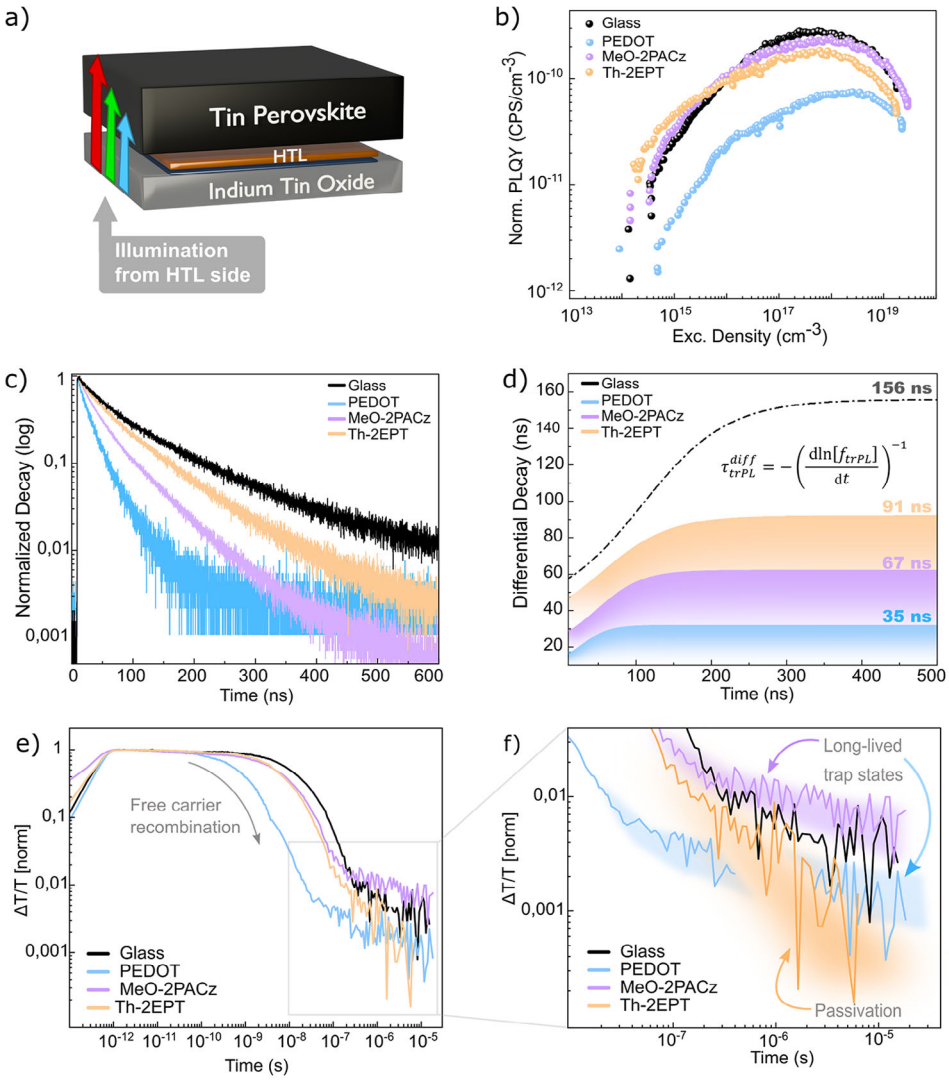

Figure 3. Optoelectronic properties. a) Schematic representation of the ITO/HTL/PVK stack on which the measurements were performed. The RGB colored arrows qualitatively represent the penetration depth dependence on the excitation wavelength. b) PLQY plots were obtained by integrating the PL spectrum as a function of excitation density. c) Normalized nanosecond-resolved photoluminescence transients (trPL) and d) computed differential lifetimes from double exponential fits to the trPL transients. e) Transient absorption (TAS) decays, showing the decay of the photo bleach peak at 850 nm, with an excitation density of $4 \cdot 10^{17}$ cm^{-3}. f) A magnified view of the TAS decay, focusing on the microseconds time range, highlights the distinct long-timescale recombination dynamics and reveals apparent differences in decay rates among the HTL substrates. Plots e) and f) only show the decay of the 850 nm peak, while full transient absorption spectra are available in Figure S5 (Supporting Information).

trPL lifetimes for Sn-based perovskites.[34,35] Following trPL, transient absorption spectroscopy (TAS) was performed. TAS measures the relative change in transmittance (photobleach) of the material as a function of time after photoexcitation. The resulting signal is proportional to the population of holes and electrons in the valence and conduction bands, respectively. The main difference of TAS with respect to trPL is that it enables tracking of both radiative and nonradiative recombination paths, while photoluminescence techniques only track radiative recombination. With a temporal resolution of ≈300 fs, TAS enables the study of excited-state dynamics across a broad time range, extending up to tens of microseconds and spanning seven orders of magnitude in resolution. For this measurement, samples were illuminated from the HTL side using a 343 nm laser, selected for its shallow penetration depth in perovskite, thereby ensuring excitation is localized near the buried interface. In Figure 3e, carrier dynamics are extracted at the photobleach maximum ≈850 nm (full spectra available in Figure S4, Supporting Information). A trend consistent with trPL is observed: the perovskite film on PEDOT exhibits the fastest decay. At the same time, those on MeO-2PACz and Th-2EPT show progressively longer lifetimes, approaching the behavior of perovskite grown on glass. Figure 3f presents the TAS decay in the microseconds range, revealing distinct decay rates for the different HTLs. The signal for Th-2EPT decays significantly faster than for PEDOT and MeO-2PACz. A rapid decay in this time window is associated with a lower density of trapped carriers, while a slower decay indicates a higher trap population. This occurs because trapped carriers sustain the TAS

© 2025 The Author(s). Advanced Energy Materials published by Wiley-VCH GmbH

16146840, 2025, 29, Downloaded from https://advanced.onlinelibrary.wiley.com/doi/10.1002/aenm.202500841 by Helmholtz-Zentrum Berlin Für, Wiley Online Library on [02/09/2025]. See the Terms and Conditions (https://onlinelibrary.wiley.com/terms-and-conditions) on Wiley Online Library for rules of use; OA articles are governed by the applicable Creative Commons License

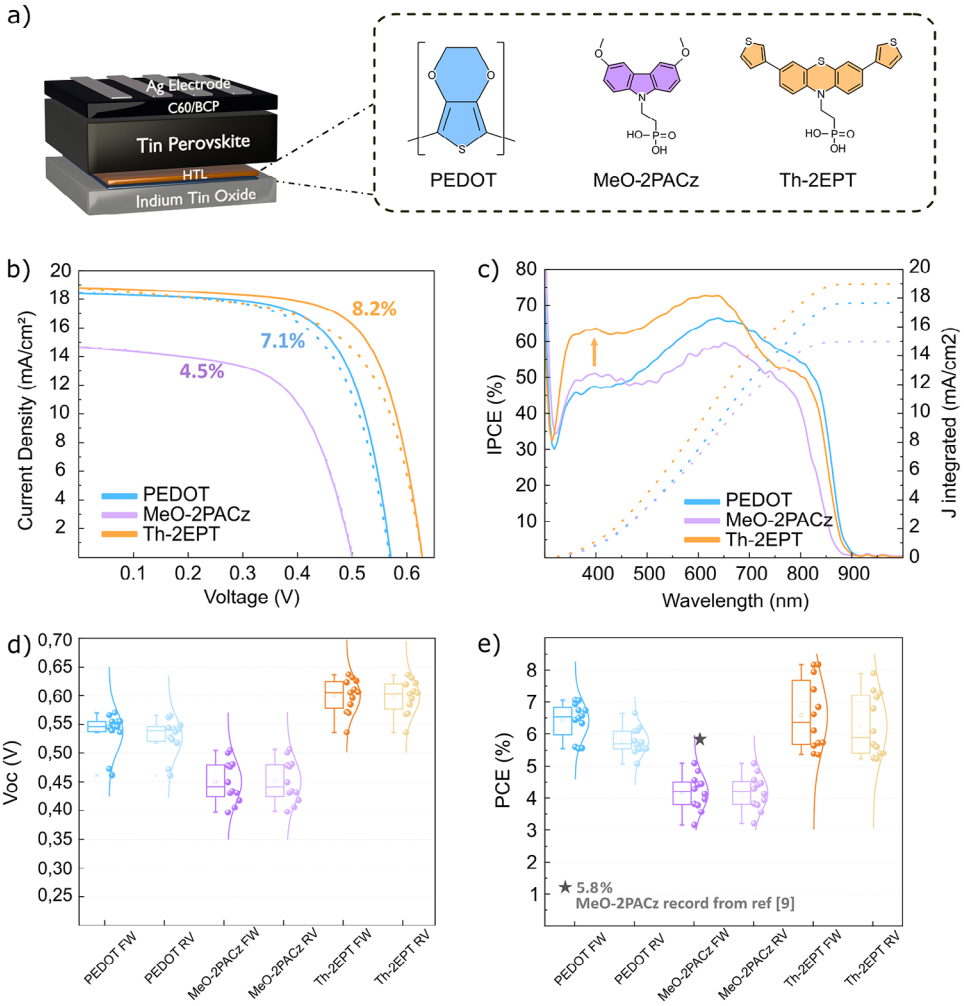

Figure 4. Solar Cell Performance. a) Schematic device structure of the lead-free solar cell used in this work (left) and molecular structures of the three different hole-selective materials (right). b) *J–V* characteristics and c) EQE spectra for the champion device for each hole-selective layer. Measured pixels in b) and c) are the same. d,e) Boxplots showing statistics for d) Open circuit voltage (V_{OC}) and e) power conversion efficiency (PCE) for the measured solar cells. Displayed with a grey star in plot e), the highest PCE was obtained with a SAM in a DMSO-free perovskite solar cell, as shown by the work of Aktas et al.[9]

signal indirectly by leaving behind an uncompensated charge in the opposite band. The longer this charge imbalance persists, the longer the signal is maintained. The fast decay observed for Th-2EPT suggests a reduced density of trapped carriers, supporting its beneficial role in defect passivation and improved interaction with the perovskite. In contrast, MeO-2PACz shows a prolonged signal, consistent with a higher trap population. In summary, PEDOT-based films exhibit short carrier lifetimes and low PLQY across all excitation densities, consistent with high nonradiative losses and poor buried interface quality. MeO-2PACz shows improved optoelectronic performance relative to PEDOT, but still exhibits signs of interfacial limitations. Both PEDOT and MeO-2PACz display prolonged TAS signals (Figure 3f), indicating long-lived trap states at the interface. Th-2EPT, by contrast, shows the slowest trPL decay, the fastest TAS signal decay in the microsecond regime, and the highest PLQY at low excitation densities—even exceeding that of glass. These results point to efficient interfacial passivation and improved carrier extraction, underscoring the effectiveness of Th-2EPT as a hole-selective interface layer for tin perovskite solar cells.

To implement improvements in optoelectronic properties and assess the impact of the SAMs on device performance, we fabricated solar cells incorporating MeO-2PACz, PEDOT, and Th-2EPT as hole-selective layers and tin perovskite $EDA_{0.05}FA_{0.95}SnI_3$ as the absorber. Our approach avoids the use of DMSO, which, despite being the most commonly used solvent for preparing tin perovskite, has also been identified as one of the sources of the Sn^{2+} oxidation.[36,37] Instead, we employed a solvent system composed of DEF (N, N'-Diethylformamide) and DMPU (N,N'-Dimethylpropyleneurea). Among the candidates, the phenothiazine-based Th-2EPT demonstrated superior performance, achieving a record efficiency of 8.2% and surpassing MeO-2PACz (4.5%) and PEDOT (7.1%). The device architecture consists of ITO/HSL/DMSO-free Sn Perovskite/C60/BCP/Ag, where the HSL was varied between the three materials. Spin-coating and dip-coating were evaluated for Th-2EPT, with

© 2025 The Author(s). Advanced Energy Materials published by Wiley-VCH GmbH

16146840, 2025, 29, Downloaded from https://advanced.onlinelibrary.wiley.com/doi/10.1002/aenm.202500841 by Helmholtz-Zentrum Berlin Für, Wiley Online Library on [02/09/2025]. See the Terms and Conditions (https://onlinelibrary.wiley.com/terms-and-conditions) on Wiley Online Library for rules of use; OA articles are governed by the applicable Creative Commons License

superior results obtained via dip-coating. The solar cell performance is summarized in **Figure 4**, which shows champion J-V curves (Figure 4b), EQE spectra (Figure 4c), V_{oc} boxplots (Figure 4d), and PCE boxplots (Figure 4e). Th-2EPT demonstrated improved short-circuit current density (J_{sc}), delivering 18.8 mA cm^{-2} compared to MeO-2PACz (14.9 mA cm^{-2}) and PEDOT (18.4 mA cm^{-2}). Incident photon current efficiency (IPCE) measurements were performed on the same champion pixels from the *J–V* measurements to investigate this improvement. The IPCE spectrum confirmed the high J_{sc} of Th-2EPT devices, with a value of 18.97 mA cm^{-2}, compared to 14.99 mA cm^{-2} for MeO-2PACz, and 17.67 mA cm^{-2} for PEDOT (Figure 4c). The EQE spectrum highlights the superior quantum efficiency of Th-2EPT, particularly at shorter wavelengths, with a high internal photon-to-electron conversion at 400 nm, far exceeding PEDOT and MeO-2PACz devices. Short wavelengths in the range 350–450 nm have low penetration depth in perovskite and are readily absorbed in the first nanometers, in the proximity of the HTL/Perovskite interface. For this reason, a substantial IPCE improvement at low wavelengths suggests improved interface quality and reduced nonradiative recombination at the Th-2EPT interface.[38] Open circuit voltage (V_{oc}) is also significantly enhanced in Th-2EPT devices compared to PEDOT and MeO-2PACz. Champion V_{oc} values of 0.63, 0.57, and 0.50 V were recorded for Th-2EPT, PEDOT, and MeO-2PACz, respectively (Figure 4d). Th-2EPT champion devices outperform PEDOT and MeO-2PACz in all solar cell parameters. Fill factor and short circuit current boxplots are shown in Figure S7 (Supporting Information). With 8.2% PCE, our Th-2EPT champion device is a record for SAM-based, DMSO-free tin perovskite solar cells to the best of our knowledge. Figure S7 (Supporting Information) presents a comparison of short-term operational stability under maximum power point (MPP) tracking of TPSC devices with different HSLs in a nitrogen environment. To gain more information on the buried interface from solar cells, we measured V_{oc} dependence on light intensity to extract the ideality factor, which quantifies deviation from ideal diode behavior, and it is a valuable index of nonradiative recombination at the interface.[39] The measurement was performed on working solar cells, displaying the same architecture used for devices, as shown in Figure 4a. While an ideal cell has $n = 1$, tin perovskite solar cells can show high ideality factors due to intense bulk and interfacial recombination.[11,40] By measuring V_{oc} across varying light intensities, the ideality factor was extracted using an equation easily derived from the diode equation in open circuit conditions:

$$n = \frac{q}{kT}\frac{dV_{oc}}{d\left(\ln(I)\right)} \tag{1}$$

The extracted values for n resulted in 2.86, 2.18, and 1.98 for MeO-2PACz, PEDOT, and Th-2EPT, respectively (**Figure 5**). The lower ideality factor with Th-2EPT is an indicator of reduced nonradiative recombination. This result confirms the ability of Th-2EPT to drastically reduce nonradiative recombination, promoting the formation of a low-defect interface through an optimized interaction.

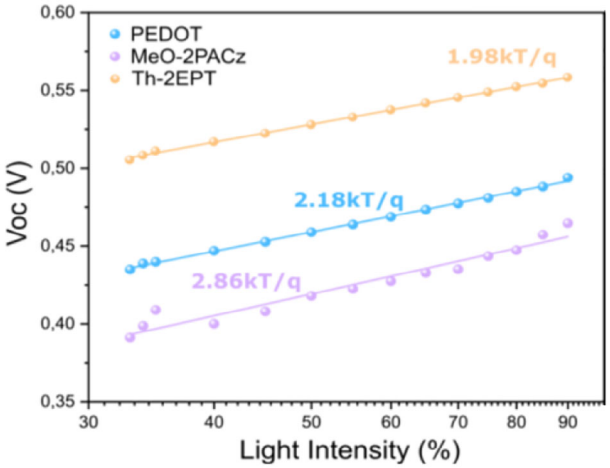

Figure 5. V_{oc} dependence on light intensity.

3. Conclusion

The majority of self-assembled monolayers (SAMs) employed as hole-selective layers in tin-based perovskite solar cells have failed to surpass the performance of PEDOT, despite its acidity, energy mismatch, and instability. In this work, we designed and synthesized a novel SAM molecule, Th-2EPT, specifically tailored to enhance lattice matching and introduce bond flexibility—addressing the limitations of MeO-2PACz. Compared to PEDOT, Th-2EPT enables the formation of perovskite films with comparable crystallinity, albeit with smaller grains. However, it delivers markedly superior optoelectronic performance. While PEDOT benefits from favorable energetic alignment with $FASnI_3$, it suffers from poor carrier dynamics, as evidenced by short lifetimes and low PLQY. In contrast, Th-2EPT demonstrates longer carrier lifetimes and higher photoluminescence efficiency, pointing to reduced nonradiative recombination. Importantly, Th-2EPT supports the fabrication of high-quality, DMSO-free devices and outperforms both PEDOT and MeO-2PACz in terms of optoelectronic quality and overall device performance. The results confirm that Th-2EPT forms an exceptionally well-passivated buried interface, effectively minimizing interfacial recombination losses. These findings establish Th-2EPT as a promising candidate for next-generation SAM-based architectures and demonstrate that rational molecular design can unlock new levels of performance in tin perovskite photovoltaics.

Supporting Information

Supporting Information is available from the Wiley Online Library or from the author.

Acknowledgements

V.S. and M.R. contributed equally to this work. This project has received funding from the Federal Ministry of Research, Technology and Space (Bundesministerium für -Forschung, Technologie und Raumfahrt) under the NanoMatFutur Call, project number 03XP0625, COMET PV, and the European Union's Framework Program for Research and Innovation HORIZON EUROPE (2021-2027) under the Marie Skłodowska-Curie

© 2025 The Author(s). Advanced Energy Materials published by Wiley-VCH GmbH

16146840, 2025, 29, Downloaded from https://advanced.onlinelibrary.wiley.com/doi/10.1002/aenm.202500841 by Helmholtz-Zentrum Berlin Für, Wiley Online Library on [02/09/2025]. See the Terms and Conditions (https://onlinelibrary.wiley.com/terms-and-conditions) on Wiley Online Library for rules of use; OA articles are governed by the applicable Creative Commons License

Action Postdoctoral Fellowships (European Fellowship) 101061809 HyPerGreen. M.M., V.G. and T.M. would like to acknowledge the project "Mission-driven Implementation of Science and Innovation Programmes" (No. 02-002-P-0001), funded by the Economic Revitalization and Resilience Enhancement Plan "New Generation Lithuania". L.F. acknowledges financial support by the German Federal Environmental Foundation (DBU). A.T., A.M. and A.A. acknowledge the Italian Ministry of Environment and Energy Security in the framework of the Project GoPV (CSEAA_00011) for Research on the Electric System. K.M. acknowledges the Gauss Centre for Supercomputing e.V. for providing computing time on the GCS Supercomputer SuperMUC-NG and the Alexander von Humboldt Foundation for the research funding.

Open access funding enabled and organized by Projekt DEAL.

Conflict of Interest

The authors declare no conflict of interest.

Data Availability Statement

The data that support the findings of this study are available from the corresponding author upon reasonable request.

Keywords

buried Interface, DMSO-free, lead-free, phenothiazine, self-assembled monolayers, solar cells, tin perovskite

Received: February 11, 2025
Revised: May 12, 2025
Published online: June 30, 2025

[1] M. Aldamasy, Z. Iqbal, G. Li, J. Pascual, F. Alharthi, A. Abate, M. Li, *Phys. Chem. Chem. Phys.* **2021**, *23*, 23413.
[2] E. Aktas, N. Rajamanickam, J. Pascual, S. Hu, M. H. Aldamasy, D. Di Girolamo, W. Li, G. Nasti, E. Martínez-Ferrero, A. Wakamiya, E. Palomares, A. Abate, *Commun. Mater.* **2022**, *3*, 104.
[3] A. Abate, *ACS Energy Lett.* **2023**, *8*, 1896.
[4] K. Dey, D. Ghosh, M. Pilot, S. R. Pering, B. Roose, P. Deswal, S. P. Senanayak, P. J. Cameron, M. S. Islam, S. D. Stranks, *Energy Environ. Sci.* **2024**, *17*, 760.
[5] A. Babayigit, D. Duy Thanh, A. Ethirajan, J. Manca, M. Muller, H.-G. Boyen, B. Conings, *Sci. Rep.* **2016**, *6*, 18721.
[6] J. Li, H.-L. Cao, W.-B. Jiao, Q. Wang, M. Wei, I. Cantone, J. Lü, A. Abate, *Nat. Commun.* **2020**, *11*, 310.
[7] Z. Le, A. Liu, Y. Reo, S. Bai, Y.-Y. Noh, H. Zhu, *ACS Energy Lett.* **2024**, *9*, 1639.
[8] G. Li, Z. Su, M. Li, F. Yang, M. H. Aldamasy, J. Pascual, F. Yang, H. Liu, W. Zuo, D. Di Girolamo, Z. Iqbal, G. Nasti, A. Dallmann, X. Gao, Z. Wang, M. Saliba, A. Abate, *Adv. Energy Mater.* **2021**, *11*, 2101539.
[9] E. Aktas, I. Poli, C. Ponti, G. Li, A. Olivati, D. Di Girolamo, F. A. Alharthi, M. Li, E. Palomares, A. Petrozza, A. Abate, *ACS Energy Lett.* **2023**, *8*, 5170.
[10] D. Cui, X. Liu, T. Wu, X. Lin, X. Luo, Y. Wu, H. Segawa, X. Yang, Y. Zhang, Y. Wang, L. Han, *Adv. Funct. Mater.* **2021**, *31*, 2100931.
[11] X. Zhang, S. Wang, W. Zhu, Z. Cao, A. Wang, F. Hao, *Adv. Funct. Mater.* **2022**, *32*, 2108832.
[12] Y. Xia, G. Yan, J. Lin, *Nanomaterials* **2021**, *11*, 3119.
[13] D. Di Girolamo, E. Aktas, C. Ponti, J. Pascual, G. Li, M. Li, G. Nasti, F. Alharthi, F. Mura, A. Abate, *Mater. Adv.* **2022**, *3*, 9083.
[14] J. Cameron, P. J. Skabara, *Mater. Horiz.* **2020**, *7*, 1759.
[15] S. Y. Kim, S. J. Cho, S. E. Byeon, X. He, H. J. Yoon, *Adv. Energy Mater.* **2020**, *10*, 2002606.
[16] M. Liu, L. Bi, W. Jiang, Z. Zeng, S.-W. Tsang, F. R. Lin, A. K.-Y. Jen, *Adv. Mater.* **2023**, *35*, 2304415.
[17] M. Azam, T. Du, Z. Wan, H. Zhao, H. Zeng, R. Wei, C. J. Brabec, J. Luo, C. Jia, *Energy Environ. Sci.* **2024**, *17*, 6974.
[18] D. Song, S. Ramakrishnan, Y. Zhang, Q. Yu, *ACS Energy Lett.* **2024**, *9*, 1466.
[19] D. Song, S. Narra, M.-Y. Li, J.-S. Lin, E. W. Diau, *ACS Energy Lett.* **2021**, *6*, 4179.
[20] X, X. Fan, W. Nie, H. Tsai, N. Wang, H. Huang, Y. Cheng, R. Wen, L. Ma, F. Yan, Y. Xia, *Adv. Sci.* **2019**, *6*, 1900813.
[21] D. Di Girolamo, E. Aktas, C. Ponti, J. Pascual, G. Li, M. Li, G. Nasti, F. Alharthi, F. Mura, A. Abate, *Mater. Adv.* **2022**, *3*, 9083.
[22] D. Liu, D. Luo, A. N. Iqbal, K. W. P. Orr, T. A. S. Doherty, Z.-H. Lu, S. D. Stranks, W. Zhang, *Nat. Mater.* **2021**, *20*, 1337.
[23] W. Jiang, Y. Hu, F. Li, F. R. Lin, A. K. Jen, *CCS Chem* **2024**, *6*, 1654.
[24] M. R. Maciejczyk, R. Chen, A. Brown, N. Zheng, N. Robertson, *J. Mater. Chem. C* **2019**, *7*, 8593.
[25] A. Ullah, K. H. Park, H. D. Nguyen, Y. Siddique, S. F. A. Shah, H. Tran, S. Park, S. I. Lee, K.-K. Lee, C.-H. Han, K. Kim, S. Ahn, I. Jeong, Y. S. Park, S. Hong, *Adv. Energy Mater.* **2022**, *12*, 2103175.
[26] H. Zhang, S. Zhang, X. Ji, J. He, H. Guo, S. Wang, W. Wu, W.-H. Zhu, Y. Wu, *Angew. Chem., Int. Ed.* **2024**, *63*, 202401260.
[27] M. Planells, A. Abate, H. J. Snaith, N. Robertson, *ACS Appl. Mater. Interfaces* **2014**, *6*, 17226.
[28] M. Liu, M. Li, Y. Li, Y. An, Z. Yao, B. Fan, F. Qi, K. Liu, H.-L. Yip, F. R. Lin, A. K.-Y. Jen, *Adv. Energy Mater.* **2024**, *14*, 2303742.
[29] X. Chen, E. Luais, N. Darwish, S. Ciampi, P. Thordarson, J. J. Gooding, *Langmuir* **2012**, *28*, 9487.
[30] S. A. Paniagua, E. L. Li, S. R. Marder, *Phys. Chem. Chem. Phys.* **2014**, *16*, 2874.
[31] D. Cui, X. Liu, T. Wu, X. Lin, X. Luo, Y. Wu, H. Segawa, X. Yang, Y. Zhang, Y. Wang, L. Han, *Adv. Funct. Mater.* **2021**, *31*, 2100931.
[32] M. Kaiser, Y. Li, I. Allegro, B. S. Richards, U. W. Paetzold, I. A. Howard, *Adv. Mater. Interfaces* **2021**, *8*, 2101326.
[33] Y. Du, Q. Tian, S. Wang, T. Yang, L. Yin, H. Zhang, W. Cai, Y. Wu, W. Huang, L. Zhang, K. Zhao, S. (F). Liu, *Adv. Mater.* **2023**, *35*, 2206451.
[34] M. Zhang, M. Zhang, P. Wang, H. Yao, C. Wu, M. Yin, H. Qiu, J. Luo, J. Du, Y. Hua, F. Hao, *Mater.* **2025**, *6*, 100425.
[35] G. Liu, X. Jiang, Y. He, C.-H. Kuan, G. Yang, W. Feng, X. Chen, W.-Q. Wu, *Angew. Chem.* **2025**, *137*, 202419183.
[36] J. Pascual, D. Di Girolamo, M. A. Flatken, M. H. Aldamasy, G. Li, M. Li, A. Abate, *Chem. – Eur. J.* **2022**, *28*, 202103919.
[37] M. I. Saidaminov, I. Spanopoulos, J. Abed, W. Ke, J. Wicks, M. G. Kanatzidis, E. H. Sargent, *ACS Energy Lett.* **2020**, *5*, 1153.
[38] N. Alias, A. Ali Umar, N. A. A. Malek, K. Liu, X. Li, N. A. Abdullah, M. M. Rosli, M. Y. Abd Rahman, Z. Shi, X. Zhang, H. Zhang, F. Liu, J. Wang, Y. Zhan, *ACS Appl. Mater. Interfaces* **2021**, *13*, 3051.
[39] P. Caprioglio, C. M. Wolff, O. J. Sandberg, A. Armin, B. Rech, S. Albrecht, D. Neher, M. Stolterfoht, *Adv. Energy Mater.* **2020**, *10*, 2000502.
[40] M. H. Aldamasy, A. Musiienko, M. Rusu, D. Regaldo, S. Zuo, H. Hampel, C. Frasca, Z. Iqbal, T. W. Gries, G. Li, E. Aktas, G. Nasti, M. Li, J. Pascual, N. T. Putri Hartono, Q. Wang, T. Unold, A. Abate, Photovoltaic potential of tin perovskites revealed through layer-by- layer investigation of optoelectronic and charge transport properties, arXiv 2023, arXiv:2309.05481 [cond-mat.mtrl-sci.

© 2025 The Author(s). Advanced Energy Materials published by Wiley-VCH GmbH

16146840, 2025, 29, Downloaded from https://advanced.onlinelibrary.wiley.com/doi/10.1002/aenm.202500841 by Helmholtz-Zentrum Berlin Für, Wiley Online Library on [02/09/2025]. See the Terms and Conditions (https://onlinelibrary.wiley.com/terms-and-conditions) on Wiley Online Library for rules of use; OA articles are governed by the applicable Creative Commons License